XI International Conference on Computational Plasticity. Fundamentals and Applications
COMPLAS XI
E. Oñate, D.R.J. Owen, D. Peric and B. Suárez (Eds)

INTERIOR-POINT ALGORITHM FOR SHAKEDOWN ANALYSIS ACCOUNTING FOR LIMITED KINEMATICAL HARDENING

JAAN-W. SIMON AND DIETER WEICHERT

Institute of General Mechanics, RWTH Aachen University
Templergraben 64, 52062 Aachen, Germany
e-mail: simon@iam.rwth-aachen.de, weichert@iam.rwth-aachen.de

Key words: Shakedown Analysis, Direct Methods, Interior-Point Algorithm, Limited Kinematical Hardening, Nonlinear Programming

Abstract. We present a numerical method for the computation of shakedown loads of structures under thermo-mechanical loading accounting for limited kinematical hardening. The method is based on the lower bound approach by Melan extended to the hardening using a two-surface model. Both the yield and the bounding surface are defined by the von Mises condition. Melan's shakedown theorem leads to a nonlinear convex optimization problem. This is solved by the interior-point algorithm IPSA recently developed by the authors. In this paper, theoretical and numerical aspects will be presented as well as numerical examples from mechanical engineering.

1 INTRODUCTION

We consider engineering structures subjected to varying thermo-mechanical loading beyond the elastic limit. For these, we determine the shakedown factor α_{SD}, which is the maximum loading factor α such that the structure does neither fail due to spontaneous or incremental collapse nor due to alternating plasticity. In this paper, this is done by means of direct methods, comprising limit and shakedown analysis. In particular, we follow the statical approach of MELAN [7], who formulated a shakedown theorem for elastic-perfectly plastic and unlimited kinematical hardening continua.

Consideration of kinematical hardening is crucial for most engineering problems and thus has been addressed by several authors in the field of shakedown analysis. Notably, accounting for only unlimited kinematical hardening does not cover incremental collapse but solely alternating plasticity, see e.g. [6, 12, 18]. Thus, it is important to take into account limited kinematical hardening for obtaining realistic results. The first explicit formulation for this was given by WEICHERT and GROSS-WEEGE [3, 17], who developed

a two-surface model, which allows an easy introduction of this phenomenon to the statical shakedown theorem [3, 10, 11, 16, 17].

Using the statical shakedown theorem leads to nonlinear convex optimization problems, which are typically characterized by large numbers of unknowns and constraints. In this work, these will be solved by the interior-point algorithm IPSA recently developed by the authors [13–15], which is extended for limited kinematical hardening.

2 STATICAL APPROACH OF SHAKEDOWN ANALYSIS

The current formulation is based on the statical shakedown theorem by MELAN [7]. This states that a structure will shake down, if there exists a time-independent residual stress field $\bar{\boldsymbol{\rho}}(\boldsymbol{x})$, such that the yield condition $f[\boldsymbol{\sigma}(\boldsymbol{x},t)] \leq 0$ is satisfied for any loading path in the considered loading domain at any time t and in any point $\boldsymbol{x}$ of the structure. For the mathematical formulation, the total stress $\boldsymbol{\sigma}(\boldsymbol{x},t)$ is decomposed into an elastic stress $\boldsymbol{\sigma}^E(\boldsymbol{x},t)$ and a residual stress $\boldsymbol{\rho}(\boldsymbol{x},t)$ induced by the evolution of plastic strains.

$$\boldsymbol{\sigma}(\boldsymbol{x},t) = \boldsymbol{\sigma}^E(\boldsymbol{x},t) + \boldsymbol{\rho}(\boldsymbol{x},t) \tag{1}$$

Here, $\boldsymbol{\sigma}^E(\boldsymbol{x},t)$ denotes the stress state, which would occur in a fictitious purely elastic reference body under the same conditions as the original one. Clearly, the residual stresses satisfy the equilibrium condition, which can be transferred to a system of linear equations using the principle of virtual work, as shown e.g. in [2].

$$\sum_{r=1}^{NG} \mathbb{C}_r \cdot \bar{\boldsymbol{\rho}}_r = \mathbf{0} \tag{2}$$

Hereby, the system has been discretized using the finite element method (FEM) and thus the stresses are approximately evaluated in the GAUSS points $r \in [1, NG]$. The equilibrium matrixes $\mathbb{C}_r$ depend on the geometry and the elementation. The kinematical boundary conditions are taken into account considering the virtual displacements to be kinematical admissible.

Let the considered body be subjected to NL varying loads. Then, the according loading domain is polyhedral with $NC = 2^{NL}$ corners. As shown in [6], it is sufficient to only consider these corners to ensure shakedown for all possible loading paths inside of the loading domain. Then, introducing the loading factor $\alpha > 0$, Melan's statical shakedown theorem can be formulated as an optimization problem:

$$(\mathcal{P}_{Melan}) \qquad \alpha_{SD} = \max \alpha$$

$$\sum_{r=1}^{NG} \mathbb{C}_r \cdot \bar{\boldsymbol{\rho}}_r = \mathbf{0} \tag{3a}$$

$$f\left(\alpha\, \boldsymbol{\sigma}_r^{E,j} + \bar{\boldsymbol{\rho}}_r, \sigma_{Y,r}\right) \leq 0\,, \quad \forall j \in [1, NC],\ \forall r \in [1, NG] \tag{3b}$$

3 CONSIDERATION OF LIMITED KINEMATICAL HARDENING

In order to take into account the limited kinematical hardening we use the two-surface model proposed by Weichert and Gross-Weege [17]. The kinematical hardening is considered as a rigid body motion of the yield surface in stress space, which is described by the six-dimensional vector of back-stresses $\boldsymbol{\pi}$ representing the translation of the yield surface's center, Fig. 1. Through the introduction of a second surfaces corresponding to the ultimate stress σ_H, the motion of the yield surface is bounded.

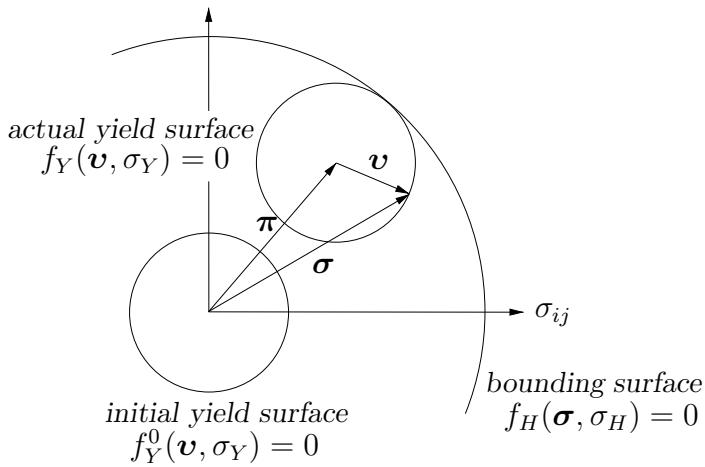

Figure 1: Kinematic hardening considered as translation of the yield surface in stress space

Thereby, the total stresses are divided into the back stresses $\boldsymbol{\pi}$ and the reduced stresses $\boldsymbol{\upsilon}$, which are responsible for the occurrence of plastic strains.

$$\boldsymbol{\sigma}(\boldsymbol{x}, t) = \boldsymbol{\pi}(\boldsymbol{x}, t) + \boldsymbol{\upsilon}(\boldsymbol{x}, t) \tag{4}$$

As before, the total stresses are decomposed, $\boldsymbol{\sigma}_r^j = \alpha\, \boldsymbol{\sigma}_r^{E,j} + \bar{\boldsymbol{\rho}}_r$. In an analogous manner, the reduced stresses $\boldsymbol{\upsilon}_r^j$ can be formulated, keeping in mind that the back stresses are time-independent and thus not dependent on the considered corner j of the loading domain, because the bounding surface is fixed in stress space.

$$\boldsymbol{\upsilon}_r^j = \boldsymbol{\sigma}_r^j - \bar{\boldsymbol{\pi}}_r = \alpha\, \boldsymbol{\sigma}_r^{E,j} + \bar{\boldsymbol{\rho}}_r - \bar{\boldsymbol{\pi}}_r \tag{5}$$

Thereby, Melan's theorem accounting for limited kinematical hardening reads as follows.

$(\mathcal{P}^H_{Melan})$ $\quad \alpha_{SD} = \max \alpha$

$$\sum_{r=1}^{NG} \mathbb{C}_r \cdot \bar{\boldsymbol{\rho}}_r = \mathbf{0} \tag{6a}$$

$$f_H\left(\alpha\, \boldsymbol{\sigma}_r^{E,j} + \bar{\boldsymbol{\rho}}_r, \sigma_{H,r}\right) \leq 0\,, \quad \forall j \in [1, NC],\ \forall r \in [1, NG] \tag{6b}$$

$$f_Y\left(\alpha\, \boldsymbol{\sigma}_r^{E,j} + \bar{\boldsymbol{\rho}}_r - \bar{\boldsymbol{\pi}}_r, \sigma_{Y,r}\right) \leq 0\,, \quad \forall j \in [1, NC],\ \forall r \in [1, NG] \tag{6c}$$

4 SOLUTION WITH INTERIOR-POINT METHOD

For a clear presentation, the problem is rewritten in the following form. To achieve this, several transformations are necessary, which are not in the scope of this paper but can be followed in [13, 15].

$$
\begin{aligned}
(\mathcal{P}_{IP}^{H}) \qquad & \min f(\boldsymbol{x}) = -\alpha \\
& \boldsymbol{A}_H \cdot \boldsymbol{x} = \boldsymbol{0} && \text{(7a)} \\
& \boldsymbol{c}_H(\boldsymbol{x}) \geq \boldsymbol{0} && \text{(7b)} \\
& \boldsymbol{c}_Y(\boldsymbol{x}) \geq \boldsymbol{0} && \text{(7c)} \\
& \boldsymbol{x} \in \mathbb{R}^n \,, && \text{(7d)}
\end{aligned}
$$

The problem $(\mathcal{P}_{IP}^{H})$ consists of n variables, merged to the solution vector $\boldsymbol{x}$, m_E equality constraints, represented by the affine linear system (7a), and $2\,m_I$ nonlinear concave inequality constraints (7b) and (7c). The equality constraints can be interpreted as equilibrium condition for the residual stresses (2), whereas the inequality constraints represent the yield and the bounding condition (6b) and (6c), respectively. The inequality constraints are converted into equality constraints by introducing slack variables $\boldsymbol{w}_H \in \mathbb{R}^{m_I}$ and $\boldsymbol{w}_Y \in \mathbb{R}^{m_I}$. Moreover, we use split variables $\boldsymbol{y} \in \mathbb{R}^n$ and $\boldsymbol{z} \in \mathbb{R}^n$ in order to avoid numerical instabilities due to the unboundedness of the solution vector (7d). Then, we use the interior-point method perturbing the objective function by logarithmic barrier terms, which penalize directions leading outside of the feasible region. Thereby, the barrier parameter μ is introduced, which is tending to zero during the iteration.

$$
f_\mu(\boldsymbol{x}, \boldsymbol{y}, \boldsymbol{z}, \boldsymbol{w}_H, \boldsymbol{w}_Y) = f(\boldsymbol{x}) - \mu \left[\sum_{i=1}^{n} \log(y_i) + \sum_{i=1}^{n} \log(z_i) + \sum_{j=1}^{m_I} \log(w_{H,j}) + \sum_{j=1}^{m_I} \log(w_{Y,j}) \right] \tag{8}
$$

The resulting optimization problem can then be expressed as follows.

$$
\begin{aligned}
(\mathcal{P}_{\mu}^{H}) \qquad & \min f_\mu(\boldsymbol{x}, \boldsymbol{y}, \boldsymbol{z}, \boldsymbol{w}_H, \boldsymbol{w}_Y) \\
& \boldsymbol{A}_H \cdot \boldsymbol{x} = \boldsymbol{0} && \text{(9a)} \\
& \boldsymbol{c}_H(\boldsymbol{x}) - \boldsymbol{w}_H = \boldsymbol{0} && \text{(9b)} \\
& \boldsymbol{c}_Y(\boldsymbol{x}) - \boldsymbol{w}_Y = \boldsymbol{0} && \text{(9c)} \\
& \boldsymbol{x} - \boldsymbol{y} + \boldsymbol{z} = \boldsymbol{0} && \text{(9d)} \\
& \boldsymbol{w}_H > \boldsymbol{0},\ \boldsymbol{w}_Y > \boldsymbol{0},\ \boldsymbol{y} > \boldsymbol{0},\ \boldsymbol{z} > \boldsymbol{0} && \text{(9e)}
\end{aligned}
$$

Since the underlying optimization problem $(\mathcal{P}_{IP}^{H})$ is convex and regular, the Karush-Kuhn-Tucker condition is both necessary and sufficient, which states that the solution is optimal if the Lagrangian $\mathcal{L}_H$ of the problem possesses a saddle point.

$$
\begin{aligned}
\mathcal{L}_H = & f_\mu(\boldsymbol{x}, \boldsymbol{y}, \boldsymbol{z}, \boldsymbol{w}_H, \boldsymbol{w}_Y) - \boldsymbol{\lambda}_E \cdot (\boldsymbol{A}_H \cdot \boldsymbol{x}) - \boldsymbol{\lambda}_H \cdot (\boldsymbol{c}_H(\boldsymbol{x}) - \boldsymbol{w}_H) \\
& - \boldsymbol{\lambda}_Y \cdot (\boldsymbol{c}_Y(\boldsymbol{x}) - \boldsymbol{w}_Y) - \boldsymbol{s} \cdot (\boldsymbol{x} - \boldsymbol{y} + \boldsymbol{z}) \,,
\end{aligned} \tag{10}
$$

where $\boldsymbol{\lambda}_E \in \mathbb{R}^{m_E}$, $\boldsymbol{\lambda}_H \in \mathbb{R}_+^{m_I}$, $\boldsymbol{\lambda}_Y \in \mathbb{R}_+^{m_I}$ and $\boldsymbol{s} \in \mathbb{R}_+^n$ are appropriate Lagrange multipliers. Thereby, the saddle point conditions reads as follows:

$$\begin{aligned}
\boldsymbol{\nabla}_x \mathcal{L}_H =& \boldsymbol{\nabla}_x f(\boldsymbol{x}) - \boldsymbol{A}_H^T \cdot \boldsymbol{\lambda}_E - \boldsymbol{C}_H^T(\boldsymbol{x}) \cdot \boldsymbol{\lambda}_H - \boldsymbol{C}_Y^T(\boldsymbol{x}) \cdot \boldsymbol{\lambda}_Y - \boldsymbol{s} = \boldsymbol{0} && \text{(11a)}\\
\boldsymbol{\nabla}_y \mathcal{L}_H =& -\mu\, \boldsymbol{Y}^{-1} \cdot \boldsymbol{e} + \boldsymbol{s} = \boldsymbol{0} && \text{(11b)}\\
\boldsymbol{\nabla}_z \mathcal{L}_H =& -\mu\, \boldsymbol{Z}^{-1} \cdot \boldsymbol{e} - \boldsymbol{s} = \boldsymbol{0} && \text{(11c)}\\
\boldsymbol{\nabla}_{w_H} \mathcal{L}_H =& -\mu\, \boldsymbol{W}_H^{-1} \cdot \boldsymbol{e} + \boldsymbol{\lambda}_H = \boldsymbol{0} && \text{(11d)}\\
\boldsymbol{\nabla}_{w_Y} \mathcal{L}_H =& -\mu\, \boldsymbol{W}_Y^{-1} \cdot \boldsymbol{e} + \boldsymbol{\lambda}_Y = \boldsymbol{0} && \text{(11e)}\\
\boldsymbol{\nabla}_{\lambda_E} \mathcal{L}_H =& -(\boldsymbol{A}_H \cdot \boldsymbol{x}) = \boldsymbol{0} && \text{(11f)}\\
\boldsymbol{\nabla}_{\lambda_H} \mathcal{L}_H =& -(\boldsymbol{c}_H(\boldsymbol{x}) - \boldsymbol{w}_H) = \boldsymbol{0} && \text{(11g)}\\
\boldsymbol{\nabla}_{\lambda_Y} \mathcal{L}_H =& -(\boldsymbol{c}_Y(\boldsymbol{x}) - \boldsymbol{w}_Y) = \boldsymbol{0} && \text{(11h)}\\
\boldsymbol{\nabla}_s \mathcal{L}_H =& -(\boldsymbol{x} - \boldsymbol{y} + \boldsymbol{z}) = \boldsymbol{0} && \text{(11i)}
\end{aligned}$$

$$\text{where:} \qquad \boldsymbol{C}_H(\boldsymbol{x}) = \boldsymbol{c}_H(\boldsymbol{x}) \boldsymbol{\nabla}_x \in \mathbb{R}^{m_I \times n} \qquad \text{and} \qquad \boldsymbol{C}_Y(\boldsymbol{x}) = \boldsymbol{c}_Y(\boldsymbol{x}) \boldsymbol{\nabla}_x \in \mathbb{R}^{m_I \times n}$$

For consistency during the iteration, we introduce the new variable $\boldsymbol{r} = -\boldsymbol{s}$ into (11c). Both of these variables are tending to zero during the iteration. In addition, the equations (11b)–(11e) are multiplied by the matrixes $\boldsymbol{Y}$, $\boldsymbol{Z}$, $\boldsymbol{W}_H$ and $\boldsymbol{W}_Y$, respectively. Merging all variables of the problem to the vector $\boldsymbol{\Pi}$), the resulting system of optimality conditions can be expressed by the function $\boldsymbol{F}_\mu^H(\boldsymbol{\Pi})$:

$$\boldsymbol{F}_\mu^H(\boldsymbol{\Pi}) = - \begin{pmatrix}
-\boldsymbol{\nabla}_x f(\boldsymbol{x}) + \boldsymbol{A}_H^T \cdot \boldsymbol{\lambda}_E + \boldsymbol{C}_H^T(\boldsymbol{x}) \cdot \boldsymbol{\lambda}_H + \boldsymbol{C}_Y^T(\boldsymbol{x}) \cdot \boldsymbol{\lambda}_Y + \boldsymbol{s} \\
\mu\, \boldsymbol{e} - \boldsymbol{Y} \cdot \boldsymbol{S} \cdot \boldsymbol{e} \\
\mu\, \boldsymbol{e} - \boldsymbol{Z} \cdot \boldsymbol{R} \cdot \boldsymbol{e} \\
\mu\, \boldsymbol{e} - \boldsymbol{W}_H \cdot \boldsymbol{\Lambda}_H \cdot \boldsymbol{e} \\
\mu\, \boldsymbol{e} - \boldsymbol{W}_Y \cdot \boldsymbol{\Lambda}_Y \cdot \boldsymbol{e} \\
\boldsymbol{A}_H \cdot \boldsymbol{x} \\
\boldsymbol{c}_H(\boldsymbol{x}) - \boldsymbol{w}_H \\
\boldsymbol{c}_Y(\boldsymbol{x}) - \boldsymbol{w}_Y \\
\boldsymbol{x} - \boldsymbol{y} + \boldsymbol{z} \\
\boldsymbol{r} + \boldsymbol{s}
\end{pmatrix} = \boldsymbol{0} \qquad (12)$$

Equation (12) constitutes a system of nonlinear equations, which will be linearized using the NEWTON method. The variables $\boldsymbol{\Pi}_{k+1}$ of the subsequent iteration step $k+1$ are computed from the variables $\boldsymbol{\Pi}_k$ of the previous one k and the step values $\Delta\boldsymbol{\Pi}_k$:

$$\boldsymbol{\Pi}_{k+1} = \boldsymbol{\Pi}_k + \Upsilon_k\, \Delta\boldsymbol{\Pi}_k\,, \qquad (13)$$

where Υ_k denotes a matrix of damping factors, which is introduced for numerical reasons. The step values $\Delta\boldsymbol{\Pi}_k$ are determined from the following linearized system of equations.

$$\boldsymbol{J}(\boldsymbol{\Pi}_k) \cdot \Delta\boldsymbol{\Pi}_k = -\boldsymbol{\nabla}_{\Pi}\mathcal{L}_H(\boldsymbol{\Pi}_k) \tag{14}$$

$$\text{where:} \quad \boldsymbol{J}(\boldsymbol{\Pi}_k) = \boldsymbol{\nabla}_{\Pi}\mathcal{L}_H(\boldsymbol{\Pi})\,\boldsymbol{\nabla}_{\Pi}\Big|_{\boldsymbol{\Pi}=\boldsymbol{\Pi}_k}$$

The Jacobian $\boldsymbol{J}(\boldsymbol{\Pi})$ of the function $\boldsymbol{F}_{\mu}^{H}(\boldsymbol{\Pi})$ can be expressed as follows:

$$\boldsymbol{J}(\boldsymbol{\Pi}) = \begin{pmatrix} \boldsymbol{\nabla}_x^2\mathcal{L}_H & \mathbf{0} & \mathbf{0} & \mathbf{0} & \mathbf{0} & -\boldsymbol{A}_H^T & -\boldsymbol{C}_H^T(\boldsymbol{x}) & -\boldsymbol{C}_Y^T(\boldsymbol{x}) & -\boldsymbol{I}_n & \mathbf{0} \\ \mathbf{0} & \boldsymbol{S} & \mathbf{0} & \mathbf{0} & \mathbf{0} & \mathbf{0} & \mathbf{0} & \mathbf{0} & \boldsymbol{Y} & \mathbf{0} \\ \mathbf{0} & \mathbf{0} & \boldsymbol{R} & \mathbf{0} & \mathbf{0} & \mathbf{0} & \mathbf{0} & \mathbf{0} & \mathbf{0} & \boldsymbol{Z} \\ \mathbf{0} & \mathbf{0} & \mathbf{0} & \boldsymbol{\Lambda}_H & \mathbf{0} & \mathbf{0} & \boldsymbol{W}_H & \mathbf{0} & \mathbf{0} & \mathbf{0} \\ \mathbf{0} & \mathbf{0} & \mathbf{0} & \mathbf{0} & \boldsymbol{\Lambda}_Y & \mathbf{0} & \mathbf{0} & \boldsymbol{W}_Y & \mathbf{0} & \mathbf{0} \\ -\boldsymbol{A}_H & \mathbf{0} & \mathbf{0} & \mathbf{0} & \mathbf{0} & \mathbf{0} & \mathbf{0} & \mathbf{0} & \mathbf{0} & \mathbf{0} \\ -\boldsymbol{C}_H(\boldsymbol{x}) & \mathbf{0} & \mathbf{0} & \boldsymbol{I}_{m_I} & \mathbf{0} & \mathbf{0} & \mathbf{0} & \mathbf{0} & \mathbf{0} & \mathbf{0} \\ -\boldsymbol{C}_Y(\boldsymbol{x}) & \mathbf{0} & \mathbf{0} & \mathbf{0} & \boldsymbol{I}_{m_I} & \mathbf{0} & \mathbf{0} & \mathbf{0} & \mathbf{0} & \mathbf{0} \\ -\boldsymbol{I}_n & \boldsymbol{I}_n & -\boldsymbol{I}_n & \mathbf{0} & \mathbf{0} & \mathbf{0} & \mathbf{0} & \mathbf{0} & \mathbf{0} & \mathbf{0} \\ \mathbf{0} & \mathbf{0} & \mathbf{0} & \mathbf{0} & \mathbf{0} & \mathbf{0} & \mathbf{0} & \mathbf{0} & -\boldsymbol{I}_n & -\boldsymbol{I}_n \end{pmatrix} \tag{15}$$

The system (14) is reduced by successive elimination of those equations, which involve diagonal matrixes. After substituting the variables $\Delta\boldsymbol{s}$, $\Delta\boldsymbol{r}$, $\Delta\boldsymbol{y}$, $\Delta\boldsymbol{z}$, $\Delta\boldsymbol{w}_H$ and $\Delta\boldsymbol{w}_Y$, the following system remains:

$$\begin{pmatrix} -\left(\boldsymbol{\nabla}_x^2\mathcal{L}_H + \boldsymbol{E}_1\right) & \boldsymbol{A}_H^T & \boldsymbol{C}_H^T(\boldsymbol{x}) & \boldsymbol{C}_Y^T(\boldsymbol{x}) \\ \boldsymbol{A}_H & \mathbf{0} & \mathbf{0} & \mathbf{0} \\ \boldsymbol{C}_H(\boldsymbol{x}) & \mathbf{0} & \boldsymbol{E}_H & \mathbf{0} \\ \boldsymbol{C}_Y(\boldsymbol{x}) & \mathbf{0} & \mathbf{0} & \boldsymbol{E}_Y \end{pmatrix} \cdot \begin{pmatrix} \Delta\boldsymbol{x} \\ \Delta\boldsymbol{\lambda}_E \\ \Delta\boldsymbol{\lambda}_H \\ \Delta\boldsymbol{\lambda}_Y \end{pmatrix} = \begin{pmatrix} \boldsymbol{d}_1 \\ \boldsymbol{d}_2 \\ \boldsymbol{d}_3^H \\ \boldsymbol{d}_3^Y \end{pmatrix} \tag{16}$$

The right-hand side values are as follows

$$\boldsymbol{d}_1 = \boldsymbol{\nabla}_x f(\boldsymbol{x}) - \boldsymbol{A}_H^T \cdot \boldsymbol{\lambda}_E - \boldsymbol{C}_H^T(\boldsymbol{x}) \cdot \boldsymbol{\lambda}_H - \boldsymbol{C}_Y^T(\boldsymbol{x}) \cdot \boldsymbol{\lambda}_Y - \boldsymbol{s} + \boldsymbol{E}_1 \cdot \boldsymbol{b}_1 \tag{17a}$$

$$\boldsymbol{d}_2 = -\boldsymbol{A}_H \cdot \boldsymbol{x} \tag{17b}$$

$$\boldsymbol{d}_3^H = -\boldsymbol{c}_H(\boldsymbol{x}) + \mu\,\boldsymbol{\Lambda}_H^{-1} \cdot \boldsymbol{e} \tag{17c}$$

$$\boldsymbol{d}_3^Y = -\boldsymbol{c}_Y(\boldsymbol{x}) + \mu\,\boldsymbol{\Lambda}_Y^{-1} \cdot \boldsymbol{e} \tag{17d}$$

$$\text{where:} \quad \boldsymbol{b}_1 = \boldsymbol{x} + \boldsymbol{z} + \mu\left(\boldsymbol{R}^{-1} - \boldsymbol{S}^{-1}\right) \cdot \boldsymbol{e} + \boldsymbol{R}^{-1} \cdot \boldsymbol{Z} \cdot \boldsymbol{s} \tag{17e}$$

$$\boldsymbol{E}_1 = \left(\boldsymbol{S}^{-1} \cdot \boldsymbol{Y} + \boldsymbol{R}^{-1} \cdot \boldsymbol{Z}\right)^{-1} \tag{17f}$$

$$\boldsymbol{E}_H = \boldsymbol{W}_H \cdot \boldsymbol{\Lambda}_H^{-1} \tag{17g}$$

$$\boldsymbol{E}_Y = \boldsymbol{W}_Y \cdot \boldsymbol{\Lambda}_Y^{-1} \tag{17h}$$

5 NUMERICAL EXAMPLES

5.1 Open-ended pipe subjected to thermo-mechanical loading

The proposed method is applied to a thin pipe subjected to an internal pressure p and a temperature load $\Delta T = T_1 - T_0$, which vary independently of each other, Fig. 2. The pipe is assumed to be long, open-ended and thin with a ratio of radius to thickness $R/h = 10$. The material parameters are assumed to be temperature-independent. Furthermore, we only consider steady-state processes assuming that the temperature is applied sufficiently slow, and no transient thermal effects are taken into account. In addition, creep due to high temperature is not considered.

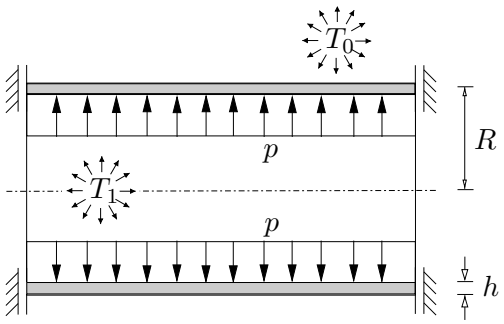

Figure 2: System of the open-ended pipe

The pipe is made of steel X6CrNiNb 18-10 and assumed to be homogeneous isotropic. The material parameters are given in Tab. 1.

Table 1: Thermal and mechanical characteristics

Young's modulus [MPa]	2.0×10^5
Yield stress [MPa]	205
Poisson's ratio	0.3
Density [kg/m^3]	7.9×10^3
Thermal conductivity [W/(m·K)]	15
Specific heat capacity [J/(kg·K)]	500
Coefficient of thermal expansion [1/K]	1.6×10^{-5}

Taking into account the symmetry of the system, the mesh consists of 984 nodes and 600 elements, where five elements over the thickness are used, Fig. 3(a). The FEM-analyses has been carried out with the software package ANSYS using isoparametric solid elements with 8 nodes. In particular, we use the element *solid45* for the structural analysis and

solid70 for the thermal one. The resulting distributions of equivalent elastic stresses are presented in Fig. 3, where the arbitrarily chosen values $p = 10$ MPa and $\Delta T = 100$ K have been used.

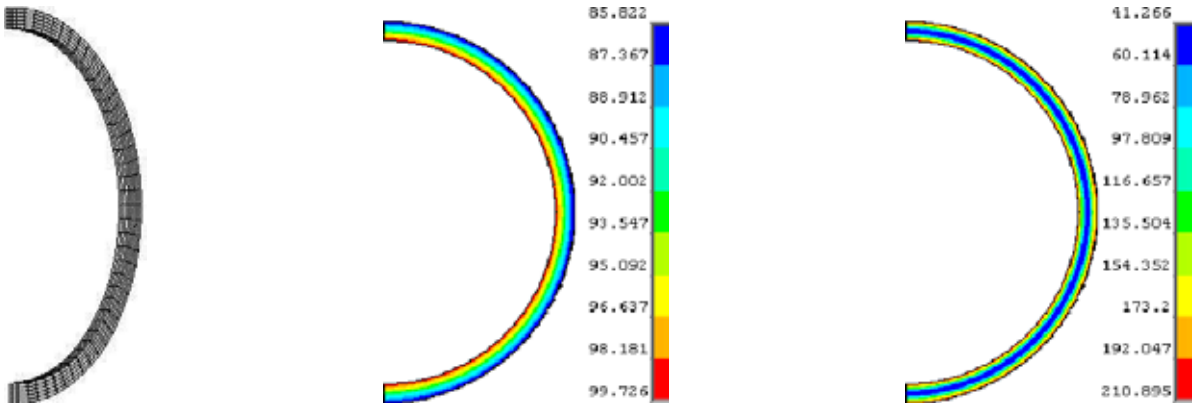

(a) FEM model

(b) Equivalent stresses due to internal pressure

(c) Equivalent stresses due to temperature loading

Figure 3: Model and elastic equivalent stresses of the open-ended pipe

The results of the shakedown analysis are presented in Fig. 4(a). There, the elastic domain (dotted line) and the shakedown curves for perfectly plastic materials as well as for limited kinematic hardening ones with different ratios $\sigma_{H,1} = 1.2\,\sigma_Y$, $\sigma_{H,2} = 1.35\,\sigma_Y$ and $\sigma_{H,3} = 1.5\,\sigma_Y$ are plotted. Both axes are scaled to the value in the perfectly plastic case p_0 and ΔT_0, respectively.

In both the perfectly plastic and the hardening case, one can clearly identify the two mechanisms of alternating plasticity and incremental collapse. In case of predominating temperature, all shakedown curves coincide with the one for unlimited hardening, which represents alternating plasticity. Here, no influence of hardening can be observed. On the other hand, failure is due to incremental collapse in the regime of predominating pressure. The limited kinematical hardening influences the shakedown curves such that the according domains increase in direct proportion with the ratio σ_H/σ_Y.

To validate the presented results, we compare them in Fig. 4 to the ones given by Mouhtamid [9], Hachemi [4] and Heitzer et al. [5]. These works are based on the static approach as well, but differ in the chosen solution strategies. Heitzer et al. applied the basis reduction technique, whereas Mouhtamid used the program Lancelot [1], which is based on the augmented Lagrangian method, and Hachemi used the bfgs algorithm, see [8]. The computed shakedown domains of Hachemi are above our ones, Fig. 4(c). The shakedown loads are overestimated in both cases with and without considering hardening. Nevertheless, the curves are qualitatively similar as well as the inclinations at the intercept points. Also, our results are in agreement with the ones of Heitzer, Fig. 4(d), which are slightly lower in the case of hardening. Furthermore, the comparison with Mouhtamid

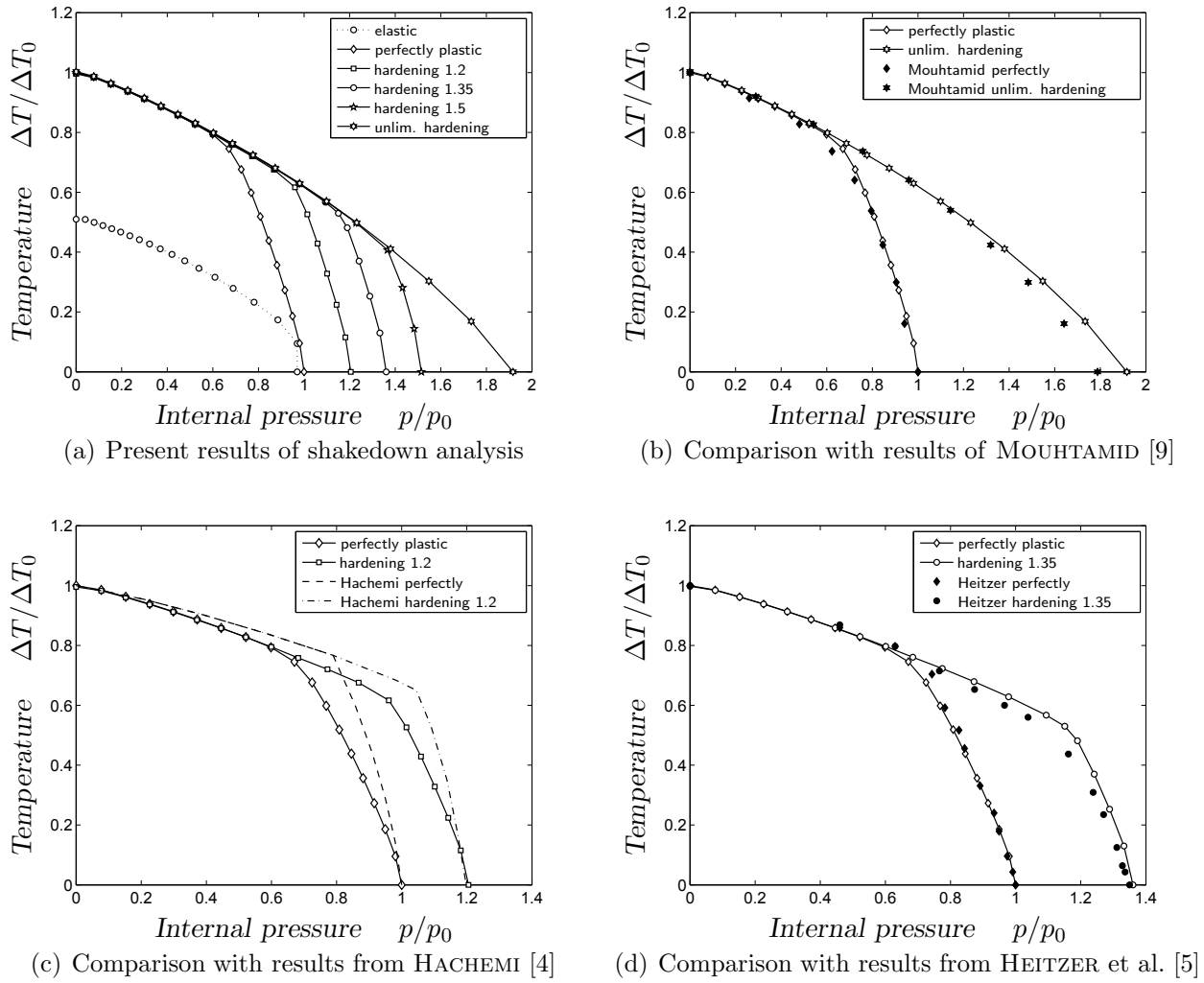

(a) Present results of shakedown analysis

(b) Comparison with results of MOUHTAMID [9]

(c) Comparison with results from HACHEMI [4]

(d) Comparison with results from HEITZER et al. [5]

Figure 4: Results of shakedown analysis and comparison to reference solutions of the open-ended pipe

shows a good agreement, too. However, a discrepancy can be observed in the regime of predominating pressure, which can be explained by different elastic solutions due to different meshes.

5.2 Closed pipe subjected to thermo-mechanical loading

For further validation, the pipe is considered now as closed, Fig. 5(a). We focus on a part of the pipe, which is far away of the closure such that local stress concentrations can be neglected. Then, the difference compared to the above calculation is the additional

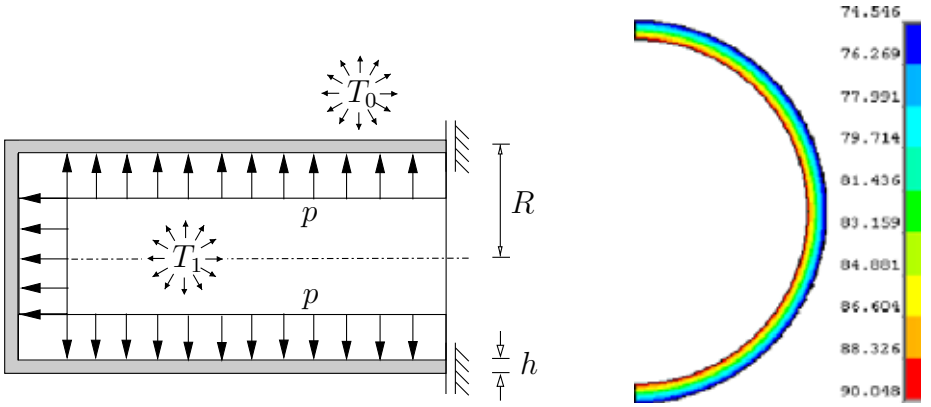

(a) System and loading conditions

(b) Equivalent stresses due to internal pressure

Figure 5: System and equivalent elastic stresses of the closed pipe

axial stress σ_{ax}, which is induced by the internal pressure acting on the cover plate.

$$\sigma_{ax} = p \frac{(R-h)^2}{(2\,R\,h - h^2)} \tag{18}$$

Through this additional axial stress the elastic stresses are changed in case of internal pressure, as shown in Fig. 5(b). As above, the value $p = 10$ MPa has been used. The elastic stresses due to the temperature loading remain as in Fig. 3(c).

The results of the shakedown analysis are presented in Fig. 4(a). There, the elastic domain (dotted line) and the shakedown curves for perfectly plastic materials as well as for limited kinematic hardening ones with different ratios $\sigma_{H,1} = 1.2\,\sigma_Y$, $\sigma_{H,2} = 1.35\,\sigma_Y$ and $\sigma_{H,3} = 1.5\,\sigma_Y$ are plotted. Both axes are scaled to the value in the perfectly plastic case p_0 and ΔT_0, respectively. Again, the two different mechanisms of alternating plasticity and incremental collapse can be clearly identified.

Finally, we compare the presented results with the ones obtained by Gross-Weege [2] using the basis reduction technique, which is based on the statical shakedown approach, too. The results are in agreement, even though in the range of incremental collapse one can observe a slight difference, Fig. 6(b).

6 CONCLUSIONS

We have presented a numerical method for shakedown analysis of engineering structures with limited kinematic hardening. The method has been implemented into the interior-point algorithm IPSA and applied to numerical examples. The validation with reference solutions is satisfying.

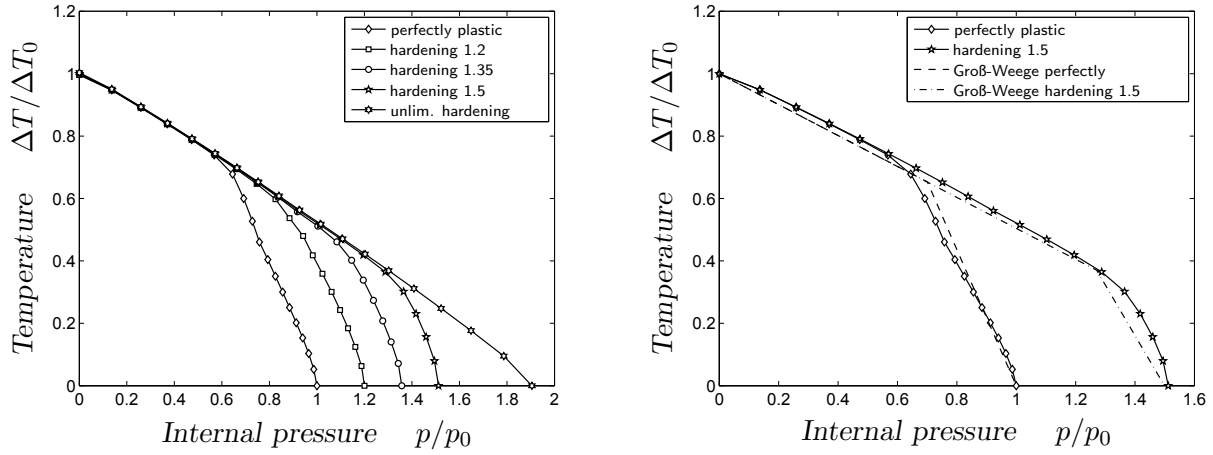

(a) Present results of shakedown analysis (b) Comparison with results of GROSS-WEEGE [2]

Figure 6: Results of shakedown analysis and comparison to reference solution of the closed pipe

REFERENCES

[1] A.R. Conn, N.I.M. Gould, and P.L. Toint. *LANCELOT: a Fortran package for large-scale nonlinear optimization (Release A)*, volume 17. Springer Series in Computational Mathematics, Springer, Heidelberg/New York, 1992.

[2] J. Groß-Weege. On the numerical assessment of the safety factor of elastic-plastic structures under variable loading. *Int J Mech Sci*, 39(4):417–433, 1997.

[3] J. Groß-Weege and D. Weichert. Elastic-plastic shells under variable mechanical and thermal loads. *Int J Mech Sci*, 34:863–880, 1992.

[4] A. Hachemi. Sur les méthodes directes et leurs applications, Habilitation, Université des Sciences et Technologies de Lille, France, 2005.

[5] M. Heitzer, G. Pop, and M. Staat. Basis reduction for the shakedown problem for bounded kinematical hardening material. *J Glob Opt*, 17:185–200, 2000.

[6] J.A. König. *Shakedown of elastic-plastic structures*. Elsevier, Amsterdam, 1987.

[7] E. Melan. Zur Plastizität des räumlichen Kontinuums. *Ing-Arch*, 9:116–126, 1938.

[8] A.J. Morris. *Foundation of Structural Optimization: A unified approach*. John Wiley, 1982.

[9] S. Mouhtamid. *Anwendung direkter Methoden zur industriellen Berechnung von Grenzlasten mechanischer Komponenten*. PhD thesis, Institute of General Mechanics, RWTH Aachen University, Germany, 2007.

[10] Q.-S. Nguyen. On shakedown analysis in hardening plasticity. *J Mech Phys Solids*, 51:101–125, 2003.

[11] P.T. Pham, D.K. Vu, T.N. Tran, and M. Staat. An upper bound algorithm for shakedown analysis of elastic-plastic bounded linearly kinematic hardening bodies. In *Proc ECCM 2010*, 2010.

[12] A.R.S. Ponter. A general shakedown theorem for elastic plastic bodies with work hardening. In *Proc SMIRT–3, paper L5/2*, 1975.

[13] J.-W. Simon, M. Chen, and D. Weichert. Shakedown analysis combined with the problem of heat conduction. In *ASME Conf Proc PVP2010*, volume 2, pages 133–142, 2010.

[14] J.-W. Simon and D. Weichert. An improved interior-point algorithm for large-scale shakedown analysis. In *PAMM – Proc Appl Math Mech*, volume 10, pages 223–224, 2010.

[15] J.-W. Simon and D. Weichert. Interior-point method for the computation of shakedown loads for engineering systems. In *ASME Conf Proc ESDA2010*, volume 4, pages 253–262, 2010.

[16] M. Staat and M. Heitzer. The restricted influence of kinematical hardening on shakedown loads. In *Proc WCCM V*, 2002.

[17] D. Weichert and J. Groß-Weege. The numerical assessment of elastic-plastic sheets under variable mechanical and thermal loads using a simplified two-surface yield condition. *Int J Mech Sci*, 30(10):757–767, 1988.

[18] J. Zarka and J. Casier. Elastic-plastic response of a structure to cyclic loading: practical rule. In S. Nemat-Nasser, editor, *Mechanics today*, volume 6. Pergamon, 1981.